

An Enhanced Generalized Average Modeling of Dual Active Bridge Converters

Liu, Bochen; Davari, Pooya; Blaabjerg, Frede

Published in:

Proceedings of 35th Annual IEEE Applied Power Electronics Conference & Exposition (APEC 2020)

DOI (link to publication from Publisher):

[10.1109/APEC39645.2020.9124001](https://doi.org/10.1109/APEC39645.2020.9124001)

Publication date:

2020

Document Version

Accepted author manuscript, peer reviewed version

[Link to publication from Aalborg University](#)

Citation for published version (APA):

Liu, B., Davari, P., & Blaabjerg, F. (2020). An Enhanced Generalized Average Modeling of Dual Active Bridge Converters. In *Proceedings of 35th Annual IEEE Applied Power Electronics Conference & Exposition (APEC 2020)* (pp. 85-90). Article 9124001 IEEE Press. <https://doi.org/10.1109/APEC39645.2020.9124001>

General rights

Copyright and moral rights for the publications made accessible in the public portal are retained by the authors and/or other copyright owners and it is a condition of accessing publications that users recognise and abide by the legal requirements associated with these rights.

- Users may download and print one copy of any publication from the public portal for the purpose of private study or research.
- You may not further distribute the material or use it for any profit-making activity or commercial gain
- You may freely distribute the URL identifying the publication in the public portal -

Take down policy

If you believe that this document breaches copyright please contact us at vbn@aub.aau.dk providing details, and we will remove access to the work immediately and investigate your claim.

An Enhanced Generalized Average Modeling of Dual Active Bridge Converters

Bochen Liu, Pooya Davari, Frede Blaabjerg

Department of Energy Technology

Aalborg University

Aalborg, Denmark

bli@et.aau.dk, pda@et.aau.dk, fbl@et.aau.dk

Abstract— An enhanced generalized average modeling (GAM) method for a dual active bridge (DAB) converter is presented in this paper. Firstly, the conventional lossless model is introduced and it is shown that this model might cause a non-neglectable steady state error. In order to improve the modeling accuracy, a wide range of loss sources are involved in the proposed enhanced GAM model, such as conduction losses and core losses. On this basis, this paper further proves that the 3rd-order harmonic component of the leakage inductance current should be considered to reduce steady state errors in light load conditions, while others might only consider the 1st-order harmonic in the existing DAB models. Also, a universal form of the modeling equation to include up to any h^{th} -order harmonic component is derived. Finally, comparative simulation and experimental results are presented to validate the feasibility of the analysis.

Keywords—generalized average modeling, dual active bridge

I. INTRODUCTION

The dual active bridge (DAB) dc-dc converter has been widely used in many applications such as distributed power systems and energy storage systems [1]–[5] due to its capabilities of matching different voltage levels and providing isolated and bidirectional power transfer. Besides, the inherent nature of zero voltage switching (ZVS) realization and simple symmetrical structure makes the DAB a potential candidate for high power density and modular applications [6], [7].

Many discrete-time models [8]–[11] of the DAB converter have been proposed to describe the converter states during different subintervals in one switching period and because of this, exact solutions for the studied state variables can be obtained. Even so, a continuous-time model is still worth researching since it can facilitate the controller design and provide an easy way to evaluate the whole system performance, especially when the DAB converter is used for modular system design.

Commonly, conventional averaging technique [12] extensively has been employed for power converter modeling. However, it requires a negligible current ripple, which is not applicable in DAB converters due to the ac transformer current. A generalized average model (GAM) [13] expands the state variables into Fourier series terms and provides a more clear representation of ac variables. Some papers [14], [15] have applied GAM to the DAB converter with focus on the tradeoff between accuracy and complexity. Of course, other methods can also be used to model the DAB converter, such as the time-domain analytical expressions based averaged

modeling presented in [16], [17] and the discrete-time models [8], [10], [11], [18]. Among the previous works, the DAB is often taken as a lossless converter or only partial losses (e.g conduction losses) are taken into account, which will result in considerable steady state errors. Another problem is that usually only the 1st-order term of the ac current is involved in the model, and this will also lead to errors especially in light load situations. On the other hand, for the time-domain analytical solution, a large amount of calculation is needed for solving the piecewise expressions in different sub-intervals, and this may become very complicated when more losses are considered.

In order to reduce the steady state error and unify the modeling procedure, an enhanced GAM for the DAB converter is presented in this paper. Various loss sources are considered in the enhanced GAM, including the conduction losses distributed on the on-state power devices, the isolating transformer and the auxiliary inductor, the core losses within the transformer and the losses from the equivalent series resistor in the DC capacitors. Besides, a universal modeling equation is derived to include up to k^{th} -order harmonic components of the leakage inductance current. For the remaining parts of this paper, the basic lossless model is firstly introduced, followed by an improved model considering power losses. In the lossy model, the steady state errors are calculated by only considering the 1st-order harmonic of the leakage inductance current, and then in order to reduce the errors in light load, the model is further improved by considering the 3rd-order harmonic component. Next, the experimental results are shown and the conclusions are summarized in the end.

II. BASIC MODEL

The commonly used lossless model of the DAB converter can be simplified as shown in Fig. 1. V_{in} is the input DC voltage, and v_p , v_s are the terminal voltages of the primary H-bridge HB₁ and secondary H-bridge HB₂, respectively. i_L is the current flowing through the leakage inductance L , which is referred to the primary side of the transformer. i_o and v_o are the output current and the output DC voltage across the resistive load R_{load} .

The single phase shift modulation is applied to the DAB converter, and the working waveforms in one switching period are shown in Fig. 1(a). φ is phase shift angle between

the voltages v_p and v_s . The diagonal power semiconductor devices in one H-bridge (e.g. S_1, S_4 in HB₁ in Fig. 1) are synchronously switched. If two switching functions $u_1(t)$ and $u_2(t)$ are introduced to HB₁ and HB₂, respectively, the following equations are satisfied.

$$\begin{aligned} u_1(t) &= \begin{cases} 1, t \in [t_0, t_2] \rightarrow S_1, S_4 \text{ on} \\ -1, t \in [t_2, t_4] \rightarrow S_2, S_3 \text{ on} \end{cases} \\ u_2(t) &= \begin{cases} 1, t \in [t_1, t_3] \rightarrow S_5, S_8 \text{ on} \\ -1, t \in [t_0, t_1] \cup (t_3, t_4] \rightarrow S_6, S_7 \text{ on} \end{cases} \end{aligned} \quad (1)$$

Then the voltages v_p and v_s can be expressed by $v_p(t) = u_1(t) \cdot V_{in}$ and $v_s(t) = u_2(t) \cdot v_o(t)$, respectively. The lossless switched model can thus be obtained.

$$\begin{cases} \frac{di_L(t)}{dt} = \frac{1}{L} u_1(t) \cdot V_{in} - \frac{n}{L} u_2(t) \cdot v_o(t) \\ \frac{dv_o(t)}{dt} = \frac{n}{C_o} u_2(t) \cdot i_L(t) - \frac{1}{R_{load} C_o} v_o(t) \end{cases} \quad (2)$$

For the convenience of derivation, $i_L(t)$, $v_o(t)$, $u_1(t)$, $u_2(t)$ in (2) are simplified with i_L , v_o , u_1 , u_2 , respectively. Focusing on the 1st-order harmonic component of the high-frequency ac current i_L and the zeroth of the output DC voltage v_o , the generalized averaged model (GAM) can be derived from (2), resulting in

$$\begin{cases} \frac{d\langle i_L \rangle_1}{dt} = -j\omega \langle i_L \rangle_1 + \frac{1}{L} \langle u_1 \rangle_1 \cdot V_{in} - \frac{n}{L} \langle u_2 \cdot v_o \rangle_1 \\ \frac{d\langle v_o \rangle_0}{dt} = \frac{n}{C_o} \langle u_2 \cdot i_L \rangle_0 - \frac{1}{R_{load} C_o} \langle v_o \rangle_0 \end{cases} \quad (3)$$

where $\omega = 2\pi f_{sw}$ (f_{sw} is the switching frequency). In order to avoid transformer saturation, the dc components of the switching functions should be zero, namely $\langle u_1 \rangle_0 = \langle u_2 \rangle_0 = 0$. Therefore, according to [13], [19], there are

$$\begin{cases} \langle u_2 \cdot v_o \rangle_1 = \langle u_2 \rangle_1 \cdot \langle v_o \rangle_0 \\ \langle u_2 \cdot i_L \rangle_0 = \langle u_2 \rangle_1 \cdot \langle i_L \rangle_{-1} + \langle u_2 \rangle_{-1} \cdot \langle i_L \rangle_1 \end{cases} \quad (4)$$

Based on (1), the 1st-order component of $u_1(t)$ and $u_2(t)$ can be calculated as

$$\langle u_1 \rangle_1 = \frac{2}{j\pi}, \quad \langle u_2 \rangle_1 = \frac{2}{j\pi} \cdot e^{-j\varphi} \quad (5)$$

Besides, for a periodic state variable x , the following relationships between the real (denoted by “R”) and imaginary (denoted by “I”) parts of $\langle x \rangle_k$ and $\langle x \rangle_{-k}$ are satisfied for the arbitrary k^{th} order coefficient.

$$\begin{cases} \langle x \rangle_{kR} = \frac{1}{T} \int_{t-T}^T x(\tau) \cos(k\omega\tau) d\tau = \langle x \rangle_{-kR} \\ \langle x \rangle_{kI} = \frac{1}{T} \int_{t-T}^T x(\tau) \sin(k\omega\tau) d\tau = -\langle x \rangle_{-kI} \end{cases} \quad (6)$$

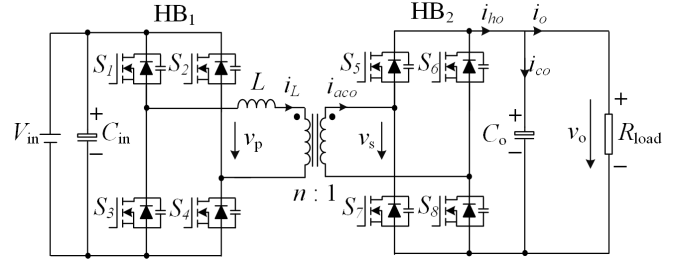


Fig. 1. Lossless DAB converter model with a resistive load.

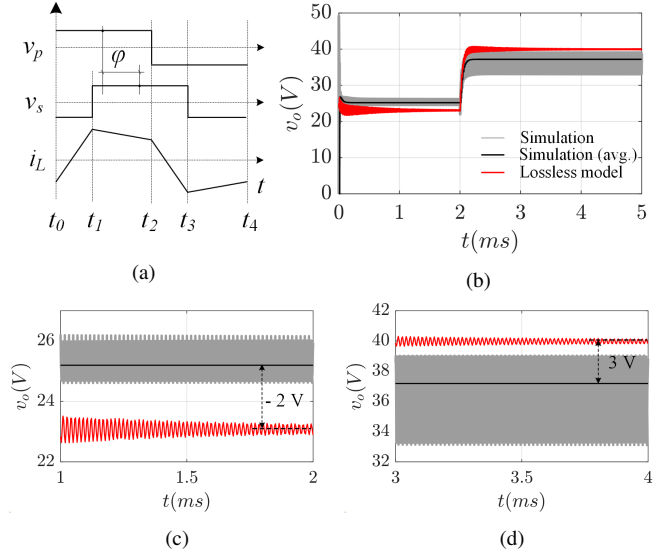


Fig. 2. Operating waveforms of the DAB converter (a) Typical working waveforms using single phase shift modulation. (b) Simulated and modeled step response by changing φ from 30° to 60° at $t=2$ ms, where the gray area is simulated v_o with switching ripples, the black solid line is the DC averaged value of the simulation results and the red is derived from (7). The corresponding simulation parameters are the same as the experiments, as listed in Table 1. (c) Zoomed area from 1 ms to 2 ms in Fig. 2(b). (d) Zoomed area from 3 ms to 4 ms in Fig. 2(b).

On the basis of (4) ~ (6), the original GAM model in (3) can be transferred to a state-space form as

$$\frac{d}{dt} \begin{bmatrix} \langle i_L \rangle_{1R} \\ \langle i_L \rangle_{1I} \\ \langle v_o \rangle_0 \end{bmatrix} = \begin{bmatrix} 0 & \omega \\ -\frac{2}{\pi L} & 0 \end{bmatrix} V_{in} + \begin{bmatrix} 0 & \omega & \frac{2n}{\pi L} \sin\varphi \\ -\omega & 0 & \frac{2n}{\pi L} \cos\varphi \\ -\frac{4n}{\pi C_o} \sin\varphi & -\frac{4n}{\pi C_o} \cos\varphi & -\frac{1}{R_{load} C_o} \end{bmatrix} \begin{bmatrix} \langle i_L \rangle_{1R} \\ \langle i_L \rangle_{1I} \\ \langle v_o \rangle_0 \end{bmatrix} \quad (7)$$

and this is the lossless generalized average model of the DAB converter, which can be directly used for parameter estimation.

In order to evaluate the accuracy of (7), a step change of the phase shift φ (switched from 30° to 60° at $t = 2$ ms) is conducted, and the resultant voltage v_o responses from the simulation and (7) are shown in Fig. 2(b). The gray area is the simulated output voltage v_o with ripples, and the solid black line is the averaged value of v_o . The solid red lines are derived from (7), which have an obvious error from the

simulated average value in both light load ($\varphi = 30^\circ$) and heavy load ($\varphi = 60^\circ$) conditions.

In order to have a clear view of the voltage errors, the waveforms during $t \in [1 \text{ ms}, 2 \text{ ms}]$ and $t \in [3 \text{ ms}, 4 \text{ ms}]$ are amplified in Fig. 2(c) and Fig. 2(d), respectively. It can be seen that there exist non-negligible errors (denoted by ΔV_{err}) between the modeling and simulated results in either light load ($\varphi = 30^\circ$, $\Delta V_{err} = -2 \text{ V}$) or heavy load ($\varphi = 60^\circ$, $\Delta V_{err} = 3 \text{ V}$). Besides, the simulated average output voltages are around 23 V and 37 V in light and heavy load, respectively, and thus the voltage error percentages in two load situations can be calculated, which are both around 8%.

III. ENHANCED GAM

As mentioned before, the commonly used lossless model is not accurate enough for estimating the output voltage in the real situation. In light of this, a new converter model considering the conduction losses, the core losses and the equivalent series resistor (ESR) of the output capacitor is built, as shown in Fig. 3(a). In the figure, the equivalent resistor R_{eq} referred to the primary side of the transformer (the turns ratio from primary to secondary side is $n : 1$) is equal to

$$R_{eq} = 2R_{DS,onP} + R_{ind} + R_{trp} + n^2 R_{trs} + n^2 R_{DS,onS} \quad (8)$$

where $R_{DS,onP}$, $R_{DS,onS}$ are the on-state resistance of each primary and secondary transistor, and R_{ind} , R_{trp} , R_{trs} are the resistance of the auxiliary inductor, the primary winding and the secondary winding of the transformer, respectively. Due to that each switch of the secondary HB₂ is composed of two paralleled transistors for reducing the current stress, the referred on-state resistance is $n^2 R_{DS,onS}$ in (8). Besides, L_M in Fig. 3(a) is the magnetic inductance and R_M is used to symbolize the core losses.

Applying a similar derivation procedure as in lossless modeling, the lossy switched model can be obtained with (9) according to the lossy converter model in Fig. 3(a).

$$\begin{cases} \frac{di_{LM}}{dt} = \frac{n}{L_M} \cdot u_2 v_o \\ i_{RM} = \frac{nu_2 v_o}{R_M} \\ i_{ho} = nu_2 \cdot (i_L - i_{RM} - i_{LM}) \\ v_o = v_{co} + R_{ESR} \cdot C_o \frac{dv_{co}}{dt} \\ \frac{dv_{co}}{dt} = \frac{i_{ho}}{C_o} - \frac{v_o}{R_{load} C_o} \\ \frac{di_L}{dt} = -\frac{R_{eq}}{L} \cdot i_L + \frac{1}{L} \cdot u_1 V_{in} - \frac{n}{L} \cdot u_2 v_o \end{cases} \quad (9)$$

From the point of unifying the i_L analysis in GAM framework, it is worth to derive a universal equation including up to the h^{th} order components. By selecting the currents flowing in the leakage inductance (i_L), magnetic inductance (i_{LM}) and the voltages across the output capacitor (v_{co}), the resistive load (v_o) as the state variables, the universal GAM equation for modeling the lossy converter can be derived in (10). Therein, the k^{th} ($k = 1, 3, 5 \dots h$) order component of i_L can be modeled by the first state-space expression, and since the magnetic current is usually much smaller than i_L , only the

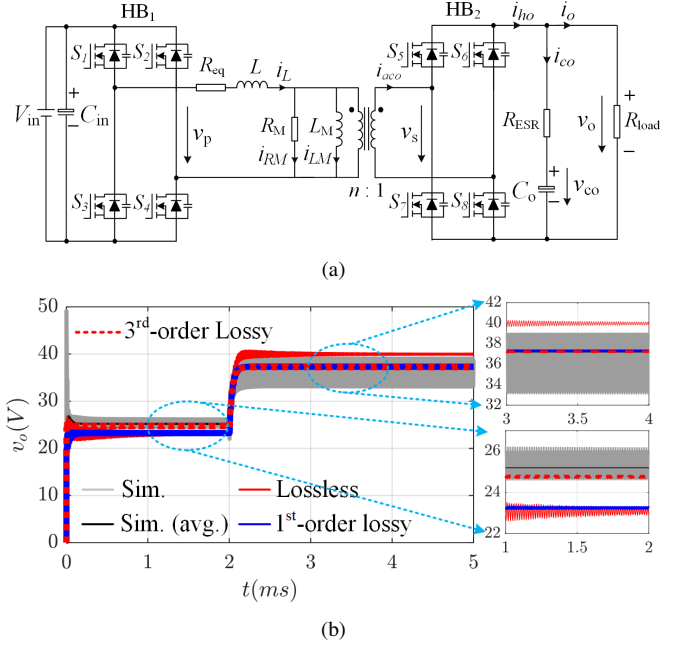


Fig. 3. Operating of the lossy DAB converter (a) Lossy DAB converter model. (b) Simulated and modeled step responses by changing φ from 30° to 60° at $t = 2 \text{ ms}$, where the gray area, the black line, the solid red line are the same as shown in Fig. 1. The blue line and the dashed red line are derived from the lossy model in (10) with $h = 1$ ($k = 1$) and $h = 3$ ($k = 1, 3$), respectively.

1^{st} order component of i_{LM} is considered, as shown by the second state-space equation. On the DAB output side, unlike the lossless converter model, the capacitor voltage v_{co} is not equal to v_o any more and the relationships between them in the GAM framework can be expressed by the last two equations in (10). The symbol C_{sys} is a coefficient of the last equation and it is constant if a DAB setup is given.

For a comparative analysis, if h in (10) is set to be 1, the 1^{st} -order lossy model can be obtained, and the resulting step response is plotted by the blue curve in Fig. 3(b). Compared to the lossless response (solid red), the 1^{st} -order lossy model (blue) results in a much smaller error from the DC averaged curve (black) in the heavy-load situation ($\varphi = 60^\circ$), as shown by the top-right inset in Fig. 3(b). Nevertheless, seen from the amplified bottom-right inset in Fig. 3(b), the resulting errors (blue) in light load ($\varphi = 30^\circ$) are almost the same as the 1^{st} -order lossless model (solid red), both having a large error from the averaged value of the output voltage (black).

This phenomenon can be explained by the following: Assuming V_{p1}/V_{s1} , V_{p3}/V_{s3} are the peak value of the 1^{st} and 3^{rd} order components of the primary and secondary voltage v_p/v_s , the transferred power through the 1^{st} and 3^{rd} order components can be approximately calculated by P_{o1} and P_{o3} , respectively, which are

$$P_{o1} = V_{p1} V_{s1} \frac{\sin \varphi}{\omega L}, \quad P_{o3} = V_{p3} V_{s3} \frac{|\sin(3\varphi)|}{3\omega L} \quad (11)$$

Considering that $V_{p3} = 1/3 V_{p1}$ and $V_{s3} = 1/3 V_{s1}$, the ratio of P_{o3}/P_{o1} will be

$$\frac{P_{o3}}{P_{o1}} = \frac{\sin(3\varphi)}{27 \cdot \sin \varphi} \quad (12)$$

Based on (12), the relationship curve between the power ration P_{o3}/P_{o1} and the phase shift φ is shown in Fig. 4. If the converter works in heavy load, taking $\varphi = 70^\circ$ as an example, the resulting ratio is 2%, which can be neglected and it indicates that the 1st-order modeling is accurate enough for heavy load situations (for the $\varphi = 60^\circ$ in Fig. 3(b) and the ratio P_{o3}/P_{o1} even becomes zero). However, in light load situations, the ratio sharply increases to 7.4% with $\varphi = 30^\circ$. Furthermore, if φ continually decreases so that $\sin\varphi \approx \varphi$ and $\sin(3\varphi) \approx 3\varphi$ are satisfied, the maximum P_{o3}/P_{o1} will reach 11%. In this case, the 3rd-order component can not be neglected, and this also is the reason why the 1st-order lossy modeling in Fig. 3(b) can help improve the heavy load performance, but has little effect in the light load.

In order to verify the theoretical analysis above, the modeled 3rd-order response is also depicted by the dashed red line in Fig. 3(b), which is obtained with $h = 3$ in (10). It can be seen from the two right insets in Fig. 3(b) that compared to the lossless model (solid red) and the 1st-order lossy model (blue), the 3rd-order model can achieve much smaller errors in both light-load and heavy-load situations. Especially, the error between the 3rd-order lossy model (blue) and the averaged simulation results (black) in light load is considerably reduced.

IV. EXPERIMENTAL VALIDATION

A test platform shown in Fig. 5 is built. The converter parameters are listed in Table I, where T_{dead} is the dead time for the two transistors in the same leg and the subscripts “ind”, “trp”, “trs” denote the auxiliary inductor, the primary and secondary winding of the transformer, respectively. The leakage inductance referred to the primary side can be calculated by $L = L_{ind} + L_{trp} + n^2 L_{trs}$. Besides, the measured (or obtained from the data sheet) parameters of the passive components and the power devices are listed in Table II.

The step responses by switching the phase shift φ between 30° and 60° are illustrated in Fig. 6, including the step-up

TABLE I
SYSTEM SPECIFICATIONS

Parameters	Description	Value
P	Rating power	1.5 kW
V_{in}	Input DC voltage	120 V
$n : 1$	Turns ratio of the transformer	3.5 : 1
f_{sw}	Switching frequency	60 kHz
T_{dead}	Dead time	400 ns
L_{ind}	Auxiliary inductor	36.2 μ H
L_{trp}	Primary-side leakage inductance	4.5 μ H
L_{trs}	Secondary-side leakage inductance	372.5 nH

TABLE II
COMPONENT PARAMETERS OF THE IMPLEMENTED PROTOTYPE

Components	Parameters
Auxiliary inductor: 10 turns Litz wire, 20 strands, 0.355 mm	$R_{ind} = 27.9 \text{ m}\Omega$ @ $T_a = 25^\circ \text{C}$
Primary winding of the DAB HF transformer: 35 turns copper foil	$R_{trp} = 607.9 \text{ m}\Omega$ @ $T_a = 25^\circ \text{C}$
Secondary winding of the DAB HF transformer: 10 turns copper foil	$R_{trs} = 16.5 \text{ m}\Omega$ @ $T_a = 25^\circ \text{C}$
Magnetic inductance of the transformer	$L_M = 1.4 \text{ mH}$
Core losses resistance	$R_M = 2 \text{ k}\Omega$ @ $T_a = 25^\circ \text{C}$
MOSFETs $S_1 \sim S_4$: IPW65R080CFD	$R_{DS, onp} = 72 \text{ m}\Omega$ @ $T_j = 25^\circ \text{C}$
MOSFETs $S_5 \sim S_8$: 2 x IPP110N20N3 in parallel	$R_{DS, ons} = 9.6 \text{ m}\Omega$ @ $T_j = 25^\circ \text{C}$
Resistive load	$R_{load} = 2.3 \Omega$
Output capacitor C_o : 2 x EETEE2D301HJ in parallel	$R_{ESR} = 30 \text{ m}\Omega$ @ $T_a = 25^\circ \text{C}$

response in Fig. 6(a) and the step-down response in Fig. 6(b). Therein, v_o is the output voltage across the resistor load, v_p is the terminal voltage of the primary H-bridge and i_L is the leakage inductance current. In the step-up response, the steady

$$\left\{ \begin{aligned} \frac{d}{dt} \begin{bmatrix} \langle i_L \rangle_{kR} \\ \langle i_L \rangle_{kI} \\ \langle v_o \rangle_0 \end{bmatrix} &= \begin{bmatrix} -R_{eq}/L & k\omega & \frac{2n}{k\pi L} \sin(k\varphi) \\ -k\omega & -R_{eq}/L & \frac{2n}{k\pi L} \cos(k\varphi) \\ \theta & \theta & \ddagger \end{bmatrix} \times \begin{bmatrix} \langle i_L \rangle_{kR} \\ \langle i_L \rangle_{kI} \\ \langle v_o \rangle_0 \end{bmatrix} + \begin{bmatrix} 0 \\ 2 \\ -\frac{2}{k\pi L} \\ 0 \end{bmatrix} V_{in} \\ \frac{d}{dt} \begin{bmatrix} \langle i_{LM} \rangle_{1R} \\ \langle i_{LM} \rangle_{1I} \\ \langle v_o \rangle_0 \end{bmatrix} &= \begin{bmatrix} 0 & \omega & -\frac{2n}{\pi L_M} \sin\varphi \\ -\omega & 0 & -\frac{2n}{\pi L_M} \cos\varphi \\ \theta & \theta & \ddagger \end{bmatrix} \times \begin{bmatrix} \langle i_{LM} \rangle_{1R} \\ \langle i_{LM} \rangle_{1I} \\ \langle v_o \rangle_0 \end{bmatrix} \\ \langle v_o \rangle_0 &= \langle v_{co} \rangle_0 + R_{ESR} \cdot C_o \frac{d}{dt} \langle v_{co} \rangle_0, \quad C_{sys} = \frac{R_M R_{load}}{(n^2 R_{ESR} + R_M) R_{load} + R_M R_{ESR}} \\ \frac{d}{dt} \langle v_{co} \rangle_0 &= \frac{C_{sys}}{C_o} \left[\frac{-4n}{\pi} \sum_{k=1,3,5..}^h \frac{\langle i_L \rangle_{kR} \sin(k\varphi) + \langle i_L \rangle_{kI} \cos(k\varphi)}{k} + \right. \\ &\quad \left. \frac{4n}{\pi} (\langle i_{LM} \rangle_{1R} \sin\varphi + \langle i_{LM} \rangle_{1I} \cos\varphi) - \left(\frac{n^2}{R_M} + \frac{1}{R_{load}} \right) \langle v_{co} \rangle_0 \right] \end{aligned} \right. \quad (10)$$

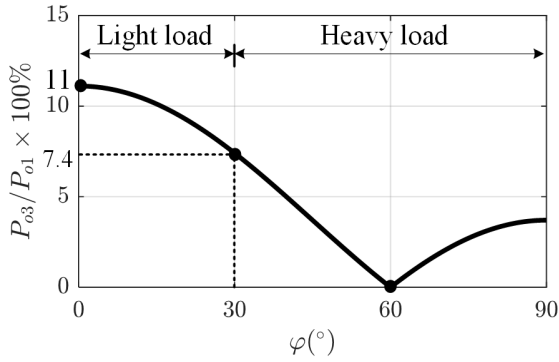


Fig. 4. Varying power ratios of the transferred power through the 3rd-order component and the 1st-order component of the leakage inductance current.

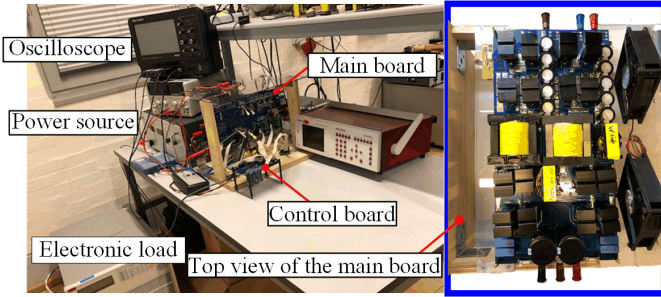


Fig. 5. Test platform for the DAB converter.

state working waveforms (as enclosed by the gray areas in Fig. 6(a)) are zoomed in Fig. 7, where v_s is the terminal voltage of the secondary H-bridge. Compared to the light load situation in Fig. 7(a), the output voltage becomes higher in Fig. 7(b) with an increased phase shift $\varphi = 60^\circ$, leading to a different shape of the leakage inductance current i_p .

In order to evaluate the modeling accuracy, the waveform data of v_o from the oscilloscope is imported to MATLAB and averaged to compare with different modeling results, as shown in Fig. 8(a). Obviously, the lossless model (denoted by the solid red line) will cause large errors from the averaged output voltage (denoted by the solid black line) in both load situations.

In order for a better view to compare the 1st-order model and the 3rd-order model, the waveforms within $[0.02s, 0.04s]$ and $[-0.03s, -0.01s]$ are amplified in Fig. 8(b) and Fig. 8(c), corresponding to the heavy load and light load, respectively. Seen from Fig. 8(b), the modeling results from the 1st-order lossy model (denoted by the solid blue line) and the 3rd-order lossy model (denoted by the dashed red line) are almost overlapped, and both achieve a more accurate result than the lossless model. Nevertheless, the 3rd-order model also can considerably improve the modeling accuracy in light load situations, where the 1st-order model has little effect and appears close to the lossless model in Fig. 8(c). These results indicate that the lossy GAM model including the 1st and 3rd components has the smallest error in both light- and heavy-load situations, which agrees well with the analysis before and signifies the correctness of the improved modeling method.

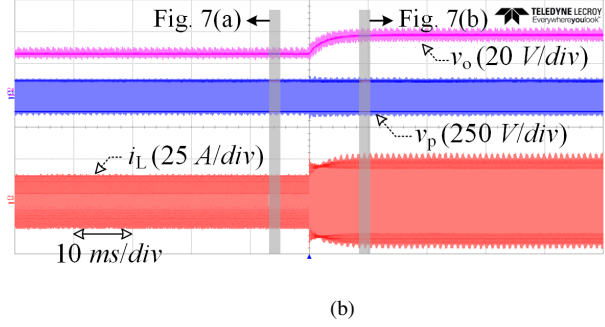
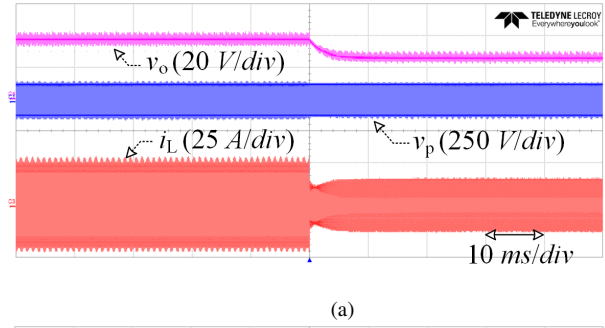


Fig. 6. Measured step response of the DAB converter: (a) with φ changing from 60° to 30° . (b) with φ changing from 30° to 60° .

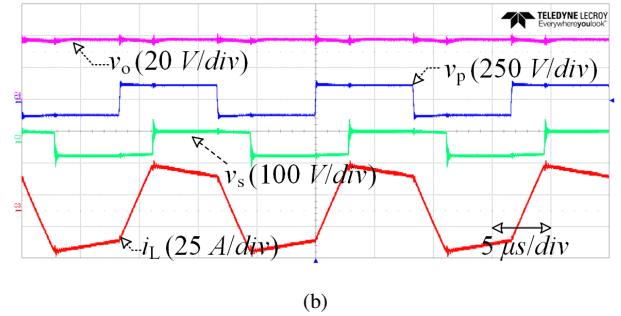
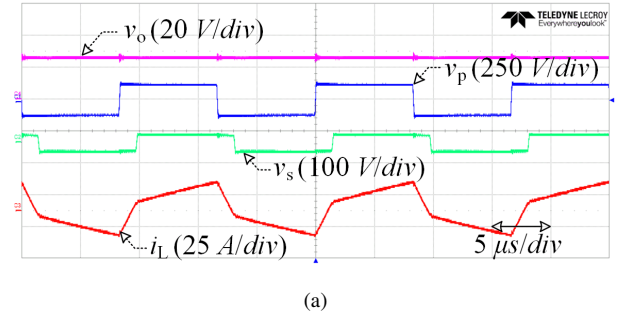


Fig. 7. Measure steady state operating waveforms of the DAB converter with (a) $\varphi = 30^\circ$. (b) $\varphi = 60^\circ$.

V. CONCLUSIONS

By involving an enhanced power loss consideration and the 3rd-order component of the ac current, the improved GAM of the DAB converter can achieve a considerably reduced steady state error compared to the conventional lossless modeling or by only considering the 1st-order term. Besides, the usage of the 3rd harmonic is emphasized in light load situations, and furthermore, a universal generalized average modeling method can be achieved by adopting the derived unified k^{th} -order model in this paper. The feasibility of the modeling analysis

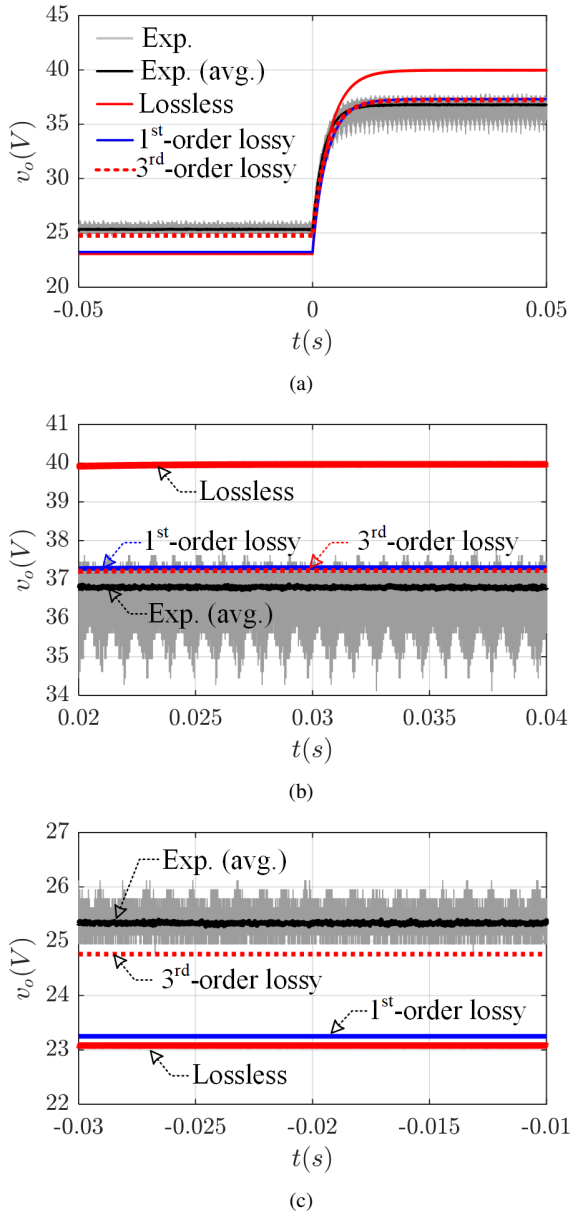


Fig. 8. Comparison of the experimental and the modeling results with a step response (a) phase shift φ changed from 30° to 60° at $t = 0$ s. (b) Zoomed-in waveforms for $t \in [0.02s, 0.04s]$ in Fig. 8(a). (c) Zoomed-in waveforms for $t \in [-0.03s, -0.01s]$ in Fig. 8(a).

is validated with simulation and experimental results.

REFERENCES

- [1] N. M. L. Tan, T. Abe, and H. Akagi, "Design and performance of a bidirectional isolated DC-DC converter for a battery energy storage system," *IEEE Trans. Power Electron.*, vol. 27, no. 3, pp. 1237–1248, 2012.
- [2] S. Inoue and H. Akagi, "A bidirectional DC-DC converter for an energy storage system with galvanic isolation," *IEEE Trans. Power Electron.*, vol. 22, no. 6, pp. 2299–2306, 2007.
- [3] B. Liu, P. Davari, and F. Blaabjerg, "A flexible control scheme for single-stage DAB AC/DC converters," in *Proc. IEEE Int. Power Electronics and Application Conf. and Exposition (PEAC)*, Nov. 2018, pp. 1–6.
- [4] Z. Wang, B. Liu, L. Guan, Y. Zhang, M. Cheng, B. Zhang, and L. Xu, "A dual-channel magnetically integrated EV chargers based on double-stator-winding permanent-magnet synchronous machines," *IEEE Trans. Ind. Appl.*, vol. 55, no. 2, pp. 1941–1953, Mar. 2019.

- [5] Z. Wang, B. Liu, Y. Zhang, M. Cheng, K. Chu, and L. Xu, "The chaotic-based control of three-port isolated bidirectional dc/dc converters for electric and hybrid vehicles," *Energies*, vol. 9, no. 2, p. 83, 2016.
- [6] B. Liu, P. Davari, and F. Blaabjerg, "An optimized control scheme for reducing conduction and switching losses in dual active bridge converters," in *Proc. IEEE Energy Conversion Congress and Exposition (ECCE)*, Sep. 2018, pp. 622–629.
- [7] B. Liu, P. Davari, and F. Blaabjerg, "An optimized control scheme to reduce the backflow power and peak current in dual active bridge converters," in *2019 IEEE Applied Power Electronics Conference and Exposition (APEC)*, IEEE, 2019, pp. 1622–1628.
- [8] C. Zhao, S. D. Round, and J. W. Kolar, "Full-order averaging modelling of zero-voltage-switching phase-shift bidirectional DC-dc converters," *IET Power Electron.*, vol. 3, no. 3, pp. 400–410, May 2010.
- [9] F. Krismer and J. W. Kolar, "Accurate small-signal model for an automotive bidirectional dual active bridge converter," in *Proc. 11th Workshop Control and Modeling for Power Electronics*, Aug. 2008, pp. 1–10.
- [10] L. Shi, W. Lei, Z. Li, J. Huang, Y. Cui, and Y. Wang, "Bilinear discrete-time modeling and stability analysis of the digitally controlled dual active bridge converter," *IEEE Trans. Power Electron.*, vol. 32, no. 11, pp. 8787–8799, Nov. 2017.
- [11] D. Costinett, "Reduced order discrete time modeling of ZVS transition dynamics in the dual active bridge converter," in *Proc. IEEE Applied Power Electronics Conference and Exposition*, Mar. 2015, pp. 365–370.
- [12] R. D. Middlebrook and S. Cuk, "A general unified approach to modelling switching-converter power stages," in *Proc. IEEE Power Electronics Specialists Conference*, Jun. 1976, pp. 18–34.
- [13] S. R. Sanders, J. M. Noworolski, X. Z. Liu, and G. C. Verghese, "Generalized averaging method for power conversion circuits," *IEEE Trans. Power Electron.*, vol. 6, no. 2, pp. 251–259, Apr. 1991.
- [14] J. A. Mueller and J. W. Kimball, "An improved generalized average model of dc-dc dual active bridge converters," *IEEE Trans. Power Electron.*, vol. 33, no. 11, pp. 9975–9988, Nov. 2018.
- [15] H. Qin and J. W. Kimball, "Generalized average modeling of dual active bridge DC-dc converter," *IEEE Trans. Power Electron.*, vol. 27, no. 4, pp. 2078–2084, Apr. 2012.
- [16] K. Zhang, Z. Shan, and J. Jatskevich, "Large-and small-signal average-value modeling of dual-active-bridge dc-dc converter considering power losses," *IEEE Trans. Power Electron.*, vol. 32, no. 3, pp. 1964–1974, Mar. 2016.
- [17] H. Bai, C. Mi, C. Wang, and S. Gargies, "The dynamic model and hybrid phase-shift control of a dual-active-bridge converter," in *Proc. 34th Annual Conf. of IEEE Industrial Electronics*, Nov. 2008, pp. 2840–2845.
- [18] F. Krismer and J. W. Kolar, "Accurate small-signal model for the digital control of an automotive bidirectional dual active bridge," *IEEE Trans. Power Electron.*, vol. 24, no. 12, pp. 2756–2768, Dec. 2009.
- [19] V. A. Caliskan, O. C. Verghese, and A. M. Stankovic, "Multifrequency averaging of DC/dc converters," *IEEE Trans. Power Electron.*, vol. 14, no. 1, pp. 124–133, Jan. 1999.